EUROFUSION WPDTT1-PR(16) 14800

F Subba et al.

Efficiency of non-standard divertor configurations in DEMO

Preprint of Paper to be submitted for publication in
22nd International Conference on Plasma Surface Interactions
in Controlled Fusion Devices (22nd PSI)

This work has been carried out within the framework of the EUROfusion Consortium and has received funding from the Euratom research and training programme 2014-2018 under grant agreement No 633053. The views and opinions expressed herein do not necessarily reflect those of the European Commission.

Title:

Preliminary analysis of the efficiency of non-standard divertor configurations in DEMO

Author names and affiliations:

[a]F. Subba, [b] L. Aho-Mantila, [c] R. Ambrosino, [d] D. P. Coster, [e] V. Pericoli-Ridolfini, [f] A. Uccello, [a] R. Zanino

[a]NEMO Group, Dipartimento Energia, Politecnico di Torino, C.so Duca degli Abruzzi 24, 10129 Torino, Italy

[b]VTT, FI-02044 Espoo, Finland

[c]Universita' degli Studi di Napoli Parthenope, Naples, Italy

[d]Max Planck Institut für Plasmaphysik, Boltzmannstraβe 2, 85748 Garching bei München, Germany

[e]Consorzio CREATE, Universitá di Napoli Federico II, Napoli, Italy

[f]Istituto di Fisica del Plasma – CNR, via R. Cozzi 53, 20125, Milano, Italy

Corresponding author:

Fabio Subba

Email: fabio.subba@polito.it

Abstract

The standard Single Null (SN) divertor is currently expected to be installed in DEMO. However, a number of alternative configurations are being evaluated in parallel as backup solutions, in case the standard divertor does not extrapolate successfully from ITER to a fusion power plant. We used the SOLPS code to produce a preliminary analysis of two such configurations, the X-Divertor (XD) and the Super X-Divertor (SXD), and compare them to the SN solution. Considering the nominal power flowing into the SOL (P_{SOL} *= 150* MW), we estimated the amplitude of the acceptable DEMO operational space. The acceptability criterion was chosen as plasma temperature at the target lower than 5 eV, providing low sputtering and at least partial detachment, while the operational space was defined in terms of the electron density at the outboard mid-plane separatrix and of the seeded impurity (Ar only in the present study) concentration. It was found that both the XD and the SXD extend the DEMO operational space, although the advantages detected so far are not dramatic. The most promising configuration seems to be the XD, which can produce acceptable target temperatures at moderate outboard mid-plane electron density ($n_{omp} = 4.5 \times 10^{19}$ m^{-3}) and Z_{eff}= 1.3.

Keywords:

DEMO, advanced divertor, numerical modeling, detachment

Introduction

The power exhaust problem in DEMO is anticipated to be considerably more challenging than in ITER. In fact, while the heating power (in DEMO mostly given by the fusion reactions) increases with the plasma volume, the available exhaust surface depends only linearly on the major radius, resulting in an unfavorable trend of the ratio P_{SOL}/R_0 of the power entering the SOL to the plasma major radius. An optimal solution would be to reduce the power flowing to the targets by radiating as much as possible from the core by means of one (or more) intentionally seeded impurity. Radiation would then distribute the exhausted power more or less uniformly over the whole first wall (FW) surface, resulting in acceptably low loads on the plasma-facing components. However, the power crossing the separatrix (P_{SOL}) cannot fall below H to L mode back transition threshold [1], to guarantee H-mode operation. For DEMO the corresponding limit is estimated to be $P_{SOL} \geq 150$ MW [2]. A large fraction of this power should be further radiated in the SOL, but the power to be handled by the divertor will still be considerable, of the order of several tens of MW [3].

The current baseline DEMO design expects to exhaust this power by means of a conventional divertor, as derived from ITER. However, alternative divertor configurations, such as the Snow Flake (SF) [4], X Divertor (XD) [5], and the Super X (SX) divertor [6] are also explored, as a backup in case the standard SN does not extrapolate favorably to a DEMO class machine. All the mentioned configurations have a potential for helping to mitigate the power exhaust problem, at the cost of increasing difficulty in engineering a proper coil system or employing efficiently the in-vessel available volume, and are under careful scrutiny during the current DEMO pre-conceptual design phase.

In this paper we perform a first comparison of the XD and SX with respect to the baseline SN (geometries are all shown in Figure 1), by means of the SOLPS5.1 package [7], excluding SF due to limitations in the current meshing capabilities of the code. At this preliminary stage of the project we want to single-out only the major differences, so we shall concentrate on the outer target, where usually the heat exhaust problem is more dramatic. We take the outboard mid-plane separatrix electron density n_{omp} (this choice mimics the experimental control on the plasma density usually obtained through gas puff) and the core-averaged Z_{eff}

(describing the amount of impurities needed to operate under given conditions) as free parameters, and try to draw the subset of the resulting operational space corresponding to acceptable plasma conditions. As acceptability criterion, we take $T < 5$ eV, which should guarantee low sputtering level (the DEMO wall material is W) and at least partial detachment.

Numerical modeling

Given the early stage of the DEMO project, it is important to produce reasonably accurate estimates of the more relevant physical quantities to guide general design decisions, as opposed to obtaining precise extensive predictions, which would depend on currently unknown machine details. Following the above considerations, the so-called reduced model approach [8] was adopted with the SOLPS-5.1 code, as a compromise between model accuracy and computational requirements. The major peculiarities of the approach are:

I. treating the neutral atoms with the fluid approximation, as opposed to the more demanding Monte Carlo (MC) EIRENE approach [7];
II. bundling the impuritiy charge states to limit the total number of simulated fluid species [9];
III. neglecting drifts in the plasma model,
IV. adopting not excessively refined (96x66) numerical meshes, based on previous extensive testing [8]; with the possible minor exception of the region very close to the targets (see e.g. Figure 9), this mesh provides smooth profiles for every quantity we checked. So we expect our results to be reasonably close to mesh independence, although we did not perform a full grid convergence analysis [10].

For all the compared configurations, we scanned a number of possible plasma conditions using as control parameters n_{ompp} and the seeded impurity level. Although in principle W could penetrate the plasma and contribute to radiation, at the low temperatures considered acceptable in our model it is not expected to produce any appreciable effect. In the SOLPS runs presented in the following, the impurity level is controlled by setting the Ar^{18+} concentration at the inner core boundary of the computational domain; however we will show our results using the more experimentally relevant Z_{eff} averaged over the plasma core (where by "core" we always mean that fraction of the confined plasma actually included in the SOLPS mesh which, for our cases, covers a fraction of the total plasma volume ranging from ~ 11% (SN) up to ~ 20% (XD)).

The operational space covered by our modeling spans approximately the region $n_{omp} = [2 \times 10^{19} - 6 \times 10^{19}]$ m^{-3}, $Z_{eff} = [1 - 2.6]$. This extends previous TECXY calculations, performed up to $n_{omp} = 4 \times 10^{19}$ m^{-3} due to code convergence problems [11]. Further TECXY analysis is discussed in [12], showing general qualitative agreement with our findings, which is not obvious since TECXY has much lower geometrical flexibility with respect to SOLPS. The upper limit for the density corresponds to about 70% of the Greenwald density or, assuming a pedestal top limit of $0.85\ n_{GW}$ [2], 82% of the pedestal density limit.

Assumed particle and heat diffusivities are $(D_\perp,\ \chi_\perp) = (0.42, 0.18)$ m^2/s, providing an e-folding length $\lambda_q \approx 3$ mm under attached conditions, compatible with predictions from the scaling presented in [13].

The neutral fluid approximation adopted should be at least marginally acceptable over the whole range of parameters explored; as a check we compared the D charge exchange and ionization mean free path for a number of cases obtained by our simulations. In the less favorable case tested ($n_{omp} = 2 \times 10^{19}$ m^{-3}, $T = 10$ eV at the target) we get $\lambda_{CX} \approx 3.3$ cm and $\lambda_{ion} \approx 6.5$ cm. Since charge-exchange processes are

effective at thermalizing the neutral distribution, this shows that the fluid approximation should be at least marginally acceptable over the whole range of parameters explored.

Results and discussion

Our main result is presented in Figure 2, which compares data from about 160 simulations for the three alternative divertor configurations here scrutinized. Each simulated shot is represented by a point in the (n_{omp}, Z_{eff}) parameter space, and is further classified according to the maximum outer target temperature. Blue marks show target temperature < 5 eV, assumed to correspond to acceptable DEMO operations. This temperature is low enough to guarantee low sputtering level, and is near to the detachment threshold. Figure 3 shows the outer target to outboard mid-plane total pressure ratio for two different densities in the LSN configuration. By detecting detachment with the onset of strong pressure drops, we see that the required temperature level is about 2 eV higher than the detachment threshold. On the other hand, since the $T < 5\ eV$ condition refers to the maximum target temperature, in most accepted cases we will have at least partial detachment. Also the peak target power flux density is strongly sensitive to the temperature near the selected threshold. On the higher T side, peak heat fluxes on target can still be as large as ~ 20 MW/m^2, dropping quickly with the temperature.

We see that, at low density, temperatures are always too high, without some amount of impurity injection. For example, for $n_{omp} = 2.5 \times 10^{19}$ m^{-3} both SN and XD require at least $Z_{eff} = 2$, although, from the simulations that were performed, we cannot determine exactly what the corresponding value for XD would be. Looking at higher densities, both SX and XD show indeed some advantage over SN. In fact, while SN needs either very large densities or high Z_{eff}, both SX and XD show low temperature at less extreme values. For example, we detected the first case for $n_{omp} = 5 \times 10^{19}$ m^{-3} (SX) or even $n_{omp} = 4.5 \times 10^{19}$ m^{-3} (XD), provided we take $Z_{eff} = 1.3$.

The previous discussion suggests that the difference among different configurations is more apparent at large densities. This is also clear from Figure 4, which shows the fraction of the heat flux reaching the outer target as a function of Z_{eff} for two different density levels. Data are distinguished according to the temperature level (below or above 5 eV) and geometry. At $n_{omp} = 2.5 \times 10^{19}$ m^{-3}, increasing the impurity content decreases the power fraction reaching the outer wall; independently of the considered divertor configuration (only SN and SX cases are available at this density). At higher n_{omp}, however, XD and SX clearly differentiate from SN. Starting from low impurity content levels, these advanced configurations detach almost immediately and drive a large fraction of the total power to the outer target. On the contrary, SN detaches only at $Z_{eff} \approx 1.5$.

We now investigate in some detail the different detachment properties of XD and SX at moderate density levels. As already noticed, for $n_{omp} = 4.5 \times 10^{19}$ m^{-3} a Z_{eff} windows exists, in which XD detaches, while SX does not. This is made apparent also by Figure 5, comparing the electron temperatures for the two geometries at $Z_{eff} \approx 1.3$. Table 1 details the distribution of cooling power in the Outer Divertor (OD) between D and Ar, making it obvious that the different Ar losses in the two cases play a significant role in XD reaching detachment.

The different role of Ar in SX vs. XD is due to a combination of two effects, related to the different connection length (from outer target to outer mid-plane) and target shape of the two configurations. Figure 6 compares the electron temperature profiles along the separatrix in the two cases. Although SX

starts from a slightly lower upstream value, this is more than compensated by the longer XD connection length, so that T_e drops below 1 eV at the target for XD, while it stays above 10 eV for SX. From the previous discussion it appears that, at least near the separatrix, the length measured along the magnetic field from the divertor region entrance up to the target is larger for XD than for SX. Figure 7 compares the distance between the divertor entrance and the target for the three configurations. We see that, close to the X-point, XD shows values larger than SX, which favors local detachment. The relation is reversed far from the strike point (SX parallel distance larger than XD), but this is less relevant, because in that region the temperatures are usually low anyway.

On top of this geometrical effect, Figure 8 shows the electron cooling rate for the different fluid species as a function of the electron temperature, while Figure 9 shows the density of the different ionic species from the outer target progressing towards outer divertor entrance along the separatrix. Instead of the perhaps more familiar distance along the separatrix, in Figure 9 we take, as independent coordinate, the electron temperature, because this gives a more direct idea about which regions are important for the cooling effects. The two configurations differ considerably in the divertor Ar^{1-17} density which, for SX, is smaller by about an order of magnitude. Moreover, it is clear from Figure 8 and Figure 9 that the super-charge state Ar^{1-17} is substantially responsible for all the Ar cooling effect (the neutral and fully ionized Ar have a density so low near outer target that they do not appear on the scale represented in the figure). Further adding to the effects discussed, we can observe from Figure 8 that most of the Ar radiation comes from a relatively narrow window centered around $T_e \approx 10$ eV. Figure 6 shows that XD, covering the whole range of temperatures down to ~ 1 eV, benefits of the whole high cooling-rate window, while SX misses about half of it, so reducing the overall cooling.

If we let the upstream density increase by about 10%, the picture changes considerably. Figure 10 shows the outer target T_e profiles for both SX and XD for almost pure D plasma, with $Z_{eff} \approx 1.03$. As we can see, in this case SX is clearly detached, while XD is not. Some light on the mechanism which produces detachment in this case is shed by Figure 11 and Figure 12, showing the behavior of the separatrix outer target density and temperature as a function of n_{omp} for the two considered configurations. Figure 11 shows that SX presents a larger sensitivity of the downstream density to the upstream value, resulting in a jump of more than a factor 5 when n_{omp} increases from 4.5×10^{19} m^{-3} to 5.0×10^{19} m^{-3}. Correspondingly, by looking at Figure 12 we see the electron temperature at the target dropping by about a factor 20. The behavior of XD is qualitatively similar, but the corresponding jump in density is smaller, and delayed at values $n_{omp} > 5.0 \times 10^{19}$ m^{-3}. Within the frame of the model adopted, this difference can be explained by the different target geometries. In fact, as shown in Figure 1, SX presents a closer configuration in comparison to XD; as a consequence, recycling neutrals are directed in a region nearer to the strike point and colder in SX than in XD, so enhancing the recycling effect itself. However, we should be aware that the fluid model adopted for the neutrals throughout this work implies a relatively poor representation of the divertor geometry. As a consequence, the appearance of effects strongly depending on such details should be confirmed by further simulations adopting the full MC model for neutral transport, which enjoys the advantage of a much more detailed divertor representation. For the time being, observations of the previously mentioned effect in favor of early SX detachment should then be taken as preliminary.

Conclusions and perspective

In this paper we presented a first, preliminary discussion of the SX and XD divertor configurations, as possible alternative solutions to the power exhaust problem in DEMO, and compared them to the baseline SN. The study was performed with the SOLPS 5.1 code and fluid neutrals, which allows including a wealth of

details of the magnetic equilibrium geometry, while accepting some simplifications in terms of wall geometry and physics details.

Our results suggest that the examined advanced divertor configurations can indeed perform better than the baseline SN, although none of them could detach the outer divertor plate at low n_{omp} without some impurity seeding (the Ar impurity in bundled charge states has been considered in the present study). At medium densities, the outer divertor detaches with some residual impurity injection (XD first), while at higher n_{omp} values outer target detachment is finally obtained even for almost pure plasma (SX first). However, the highest densities considered in this study might be too large if the currently expected pedestal top density limit is confirmed [2]. Consequently, we believe that at least some level of impurity injection will be mandatory in DEMO.

The different behavior of XD and SX has been explained with differences in the connection length (at medium density) and wall shape (at higher density). However, while the magnetic field structure is fully included in our model, the finest details of the divertor geometry are not, so that the existence of effects relying on it should be confirmed in the future by more comprehensive simulations, including the EIRENE MC model for neutral transport.

Acknowledgements:

This work has been carried out within the framework of the EUROfusion Consortium and has received funding from the EURATOM research and training programme 2014-2018 under grant agreement No 633053. The views and opinions expressed herein do not necessarily reflect those of the European Commission.

Figures

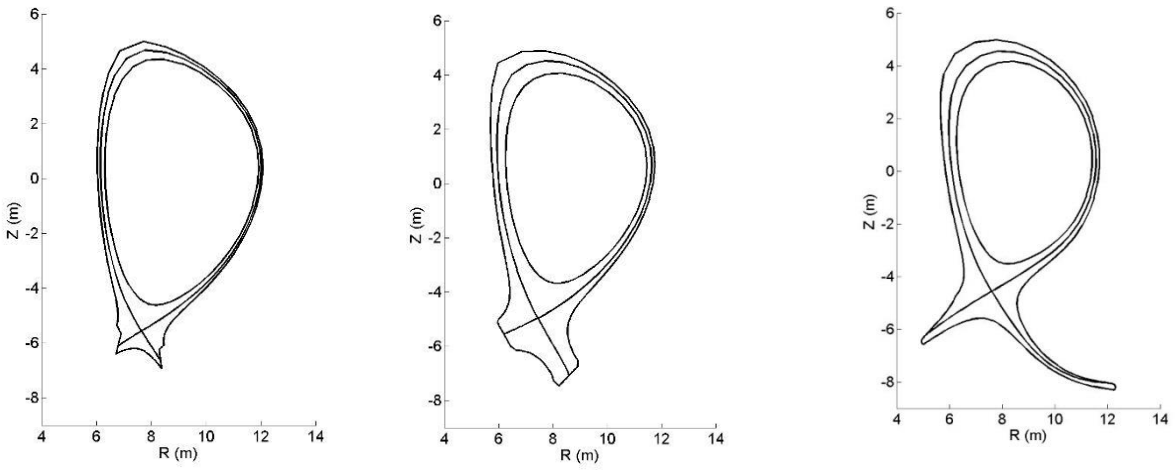

Figure 1

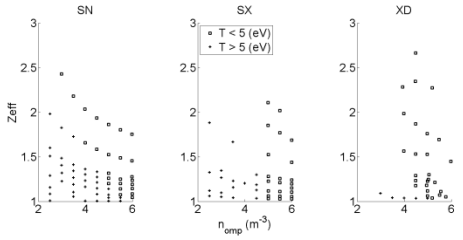

Figure 2

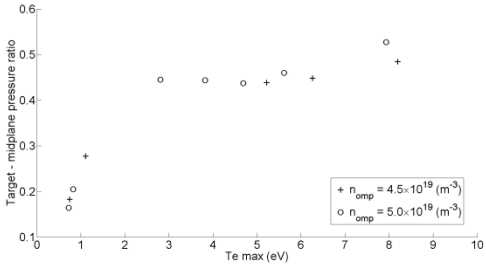

Figure 3

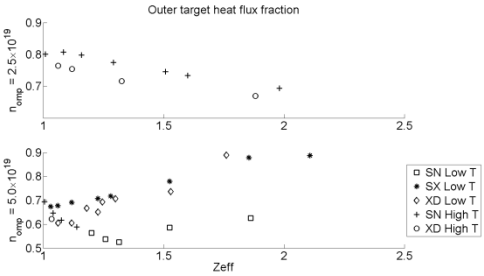

Figure 4

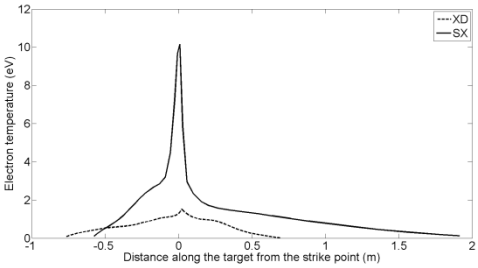

Figure 5

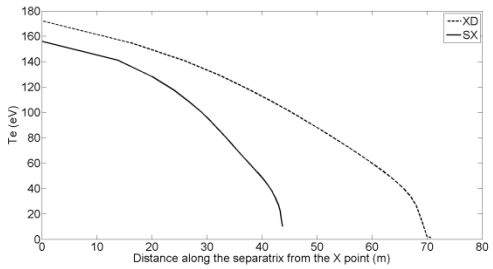

Figure 6

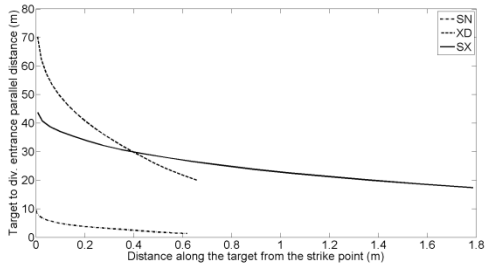

Figure 7

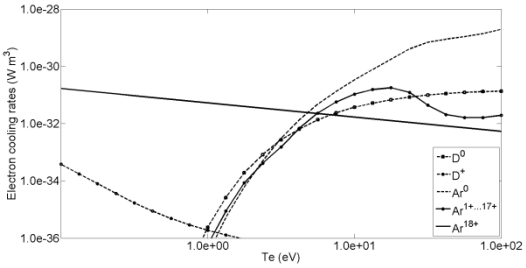

Figure 8

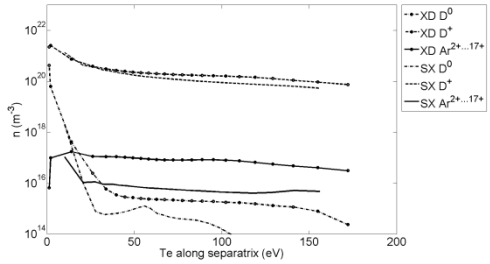

Figure 9

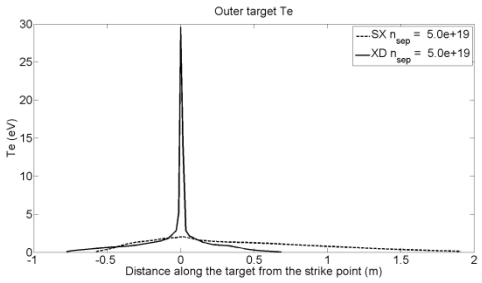

Figure 10

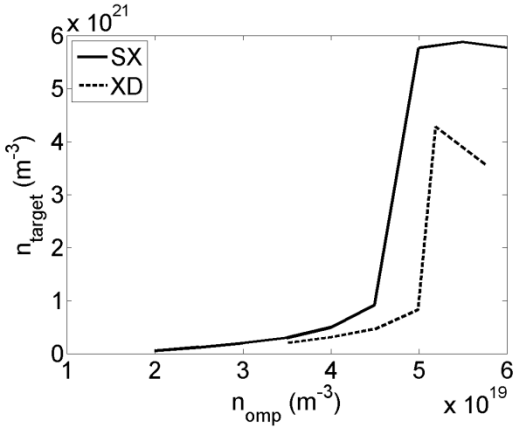

Figure 11

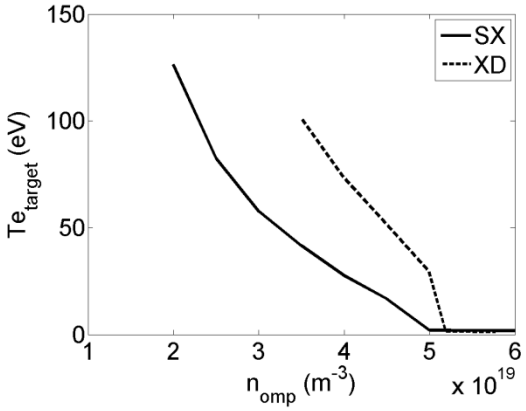

Figure 12

Tables

	SX	XD
OD cooling (total)	39 MW	50 MW
Cooling due to D	37 MW	35 MW
Cooling due to Ar	2 MW	15 MW

Table 1

Captions

Figure 1**:** Comparison of the divertor geometries considered in the paper. Left: SN, center: XD, right: SX.

Figure 2: Representation of the operational space for the three geometrical configurations analyzed. Points corresponding to temperatures lower and higher than 5 eV are distinguished.

Figure 3: Outer target-to-midplane pressure ratio at the separatrix as a function of the strike point electron temperature. Two different outer mid-plane densities are considered, showing a relative independence on this parameter.

Figure 4: Fraction of the heat flux to the targets that actually reaches the outer one, as a function of the impurity seeding level. Two different outer mid-plane densities are considered.

Figure 5: Electron temperature profiles at the outer target for XD and SX. In this case XD is detached while SX is not.

Figure 6: Electron temperature profiles along the separatrix from X-point to target. XD has a much larger connection length, which favors radiation losses and detachment.

Figure 7: Connection length from the outer mid-plane to the target at various radial positions for all the considered divertor configurations.

Figure 8: Electron cooling rates for the various species considered in our study, as a function of the electron temperature.

Figure 9**:** Density of various ionic species along the separatrix from the outer strike point towards the outer mid-plane. The electron temperature is used on the X-axis instead of the distance from the target to highlight which species can radiate more and where. Colder temperatures correspond to the target-side of the profiles.

Figure 10: Electron temperature profiles at the outer target for a low-Z, high density case. In this case SX detaches more easily than XD.

Figure 11: Electron density at the target as a function of the outer mid-plane density.

Figure 12: Electron temperature at the target, as a function of the outer mid-plane density.

Table 1: Distribution of the power volumetric losses in the outer divertor among the different atomic species for the SX and XD configurations

References

[1] Y. Martin, T. Takizuka and ITPA CDBM H-mode Database Working Group, “Power requirement for accessing the H-mode in ITER,” *Journal of Physics: Conference Series,* vol. 123, p. 012033, 2008.

[2] R. Wenninger, M. Bernert, T. Eich, E. Fable, G. Federici, A. Kallenbach, A. Loarte, C. Lowry, D. McDonald, R. Neu, T. Puetterich, P. Schneider, B. Sieglin, G. Strohmayer, F. Reimold and M. Wischmeier, "DEMO divertor limitations during and in between ELMs," *Nuclear Fusion,* vol. 54, p.

114003, 2014.

[3] R. Zagorski, V. Pericoli-Ridolfini, H. Reimerdes, R. Ambrosino, G. Calabro', P. Chmielewski, J. Harrison, I. Icanoca-Stanik, K. Lackner, T. Lunt, S. McIntosh, F. Militello, M. Poradzyski, G. Rubino, F. Subba and B. Viola, "Evaluation of the power and particle exhaust," *this conference.*

[4] D. D. Ryutov, "Geometrical properties of a “snowflake” divertor," *Physics of Plasmas,* vol. 14, no. 6, p. 064502, 2007.

[5] M. Kotschenreuther, P. Valanju, B. Covele and S. Mahajan, "Magnetic geometry and physics of advanced divertors: The X-divertor and the snowflake," *Physics of Plasmas,* vol. 20, no. 10, p. 102507, 2013.

[6] P. M. Valanju, M. Kotschenreuther and S. Mahajan, "Super X divertors for solving heat and neutron flux problems of fusion devices," *Fusion Engineering and Design,* vol. 85, pp. 46-52, 2010.

[7] R. Schneider, X. Bonnin, K. Borrass, D. Coster, H. Kastelewicz, D. Reiter, V. Rozhansky and B. Braams, "Plasma edge physics with B2-Eirene," *Contributions to Plasma Physics,* vol. 46, no. 1-2, pp. 3-191, 2006.

[8] D. Coster, "Reduced physics models in SOLPS for reactor scoping studies," *Contributions to Plasma Physics,* vol. 24, 2016.

[9] X. Bonnin, A. Kukushkin and D. P. Coster, "Code development for ITER edge modelling textendash SOLPS5.1," *Journal of Nuclear Materials,* Vols. 390-391, pp. 274-277, 2009.

[10] P. Roache, "Completed Richardson Extrapolation," *Communications in Numerical Methods in Engineering,* vol. 9, pp. 365-374, 1993.

[11] V. Pericoli-Ridolfini, H. Bufferand, G. Ciraolo, J. Harrison, T. Lunt, F. Militello, G. Pelka, G. Rubino, F. Subba, A. Uccello, B. Viola and R. Zagorski, "Summary of the AC-4 “Power exhaust modeling” achievements," Joint progress meeting of the AC activities in WPDTT1 and WPDTT2, Jan 13-14, 2016.

[12] R. Zagorski, H. Reimerdes, R. Ambrosino, H. Bufferand, G. Calabro, P. Chmielewski, G. Ciraolo, J. Harrison, I. Ivanova-Stanik, K. Lackner, T. Lunt, S. McIntosh, S. Militello, M. Poradzyński, G. Rubino, F. Subba, R. Wenninger, B. Viola and H. Zohm, "Evaluation of the power and particle and particle exhaust performance of various alternative divertor concepts for DEMO," in *22nd International Conference on Plasma Surface Interactions in Controlled Fusion Devices*, Rome, 2016.

[13] T. Eich, B. Sieglin, A. Scarabosio, W. Fundamenski, R. J. Goldston and A. Herrmann, "Inter-elm power decay length for jet and ASDEX Upgrade: Measurement and Comparison with Heuristic Drift-Based Model," *Physical Review Letters,* vol. 107, p. 215001, 2011.